

# Optical Engineering

[SPIDigitalLibrary.org/oe](http://SPIDigitalLibrary.org/oe)

## **Fermi Gamma-Ray Space Telescope**

Julie E. McEnery  
Peter F. Michelson  
William S. Paciesas  
Steven Ritz



# Fermi Gamma-Ray Space Telescope

**Julie E. McEnery**

NASA Goddard Space Flight Center  
Greenbelt, Maryland 20771  
E-mail: julie.mcenery@nasa.gov

**Peter F. Michelson**

Stanford University  
W. W. Hansen Experimental Physics Laboratory  
Stanford, California, 94305-4085

**William S. Paciesas**

University of Alabama in Huntsville, Huntsville  
Center for Space Plasma and Aeronomic  
Research (CSPAR)  
Huntsville, Alabama 35899

**Steven Ritz**

University of California  
Santa Cruz Institute for Particle Physics  
Santa Cruz, California 95064

**Abstract.** The Fermi Gamma-ray Space Telescope, launched in June 2008, is an observatory designed to survey the high-energy gamma-ray sky. The primary instrument, the Large Area Telescope (LAT), provides observations from 20 MeV to greater than 300 GeV. A second instrument, the Gamma-ray Burst Monitor (GBM), provides observations of transients from less than 10 keV to 40 MeV. We describe the design and performance of the instruments and their subsystems, the spacecraft and the ground system. © 2012 Society of Photo-Optical Instrumentation Engineers (SPIE). [DOI: 10.1117/1.OE.51.1.011012]

Subject terms: astronomy; gamma rays; silicon.

Paper 110967SS received Aug. 11, 2011; revised manuscript received Oct. 17, 2011; accepted for publication Oct. 25, 2011; published online Feb. 10, 2012.

## 1 Introduction

Gamma-rays, residing at the extreme high-energy end of the electromagnetic spectrum, reveal the most extreme environments in the universe. Unlike lower-energy X-rays, gamma-rays are not produced thermally and are, instead, directly associated with very high-energy particle acceleration and/or new high-energy particle physics processes. Thus, the gamma-ray sky looks radically different from what is seen with the eyes: in particular, the gamma-ray universe is variable on all observed timescales. The list of gamma-ray sources of great interest includes supermassive black hole systems (active galactic nuclei, AGN), gamma-ray bursts, pulsars, supernova remnants and pulsar wind nebulae, compact binary systems, novae, the sun, diffuse emissions (both from within our Milky Way galaxy and from extragalactic sources active in the early universe), as well as hypothesized emission from clusters of galaxies and from new physics processes such as interactions of massive dark matter particles.

The launch of the Fermi Gamma-ray Space Telescope in June 2008 provided a huge leap in several key capabilities. The Large Area Telescope (LAT), which covers the energy range from 20 MeV to greater than 300 GeV, has a 2.4 steradian (sr) field of view (it sees about 20 percent of the sky at any instant), so in two orbits it is possible to expose the entire sky; furthermore, because individual photon events are recorded, over time the observatory sees ever more deeply. A photon from tomorrow's observation can be added to photons from the first day of the mission, or the events over the whole mission can be divided into whatever time bins are useful for the analysis, with precision better than 1 microsecond. The other instrument, the Gamma-ray Burst Monitor (GBM), covers the complementary energy

range 8 keV–40 MeV. Thus, for bursts, Fermi can measure fluxes over seven decades of energy. With a 9 sr field of view, the GBM sees the entire sky not occulted by the earth.

The breakthrough capabilities of the LAT were made possible by the close cooperation of the high-energy astrophysics and high-energy particle physics communities—and their associated funding agencies—in the U.S., France, Italy, Japan, and Sweden. The GBM was the result of close cooperation between the U.S. and Germany. The LAT and GBM international instrument teams continue to play critical roles in the operation of the mission.

Another important feature of the mission is the immediate release of data without proprietary period: since September 2009, the measured quantities associated with LAT photons are available on the web typically within 10 hours. Software tools jointly developed by the instrument teams and the Fermi Science Support Center [FSSC, at NASA Goddard Space Flight Center (GSFC)], along with documentation and worked examples, are also provided.

Science data are transmitted from the observatory to the Mission Operations Center (MOC) at GSFC via the Tracking and Data Relay Satellite (TDRS) System, and are quickly forwarded to the Instrument Operations Centers at SLAC (LAT) and in Huntsville (GBM), where they are processed. Data products are delivered to the FSSC for immediate distribution to the scientific community via the HEASARC data archive facility.

Fermi science operations have been extremely successful; the instrument teams have published more than 100 papers, with hundreds more published by guest observers and users. Figure 1 shows a map of the sky, in Galactic coordinates, above 1 GeV using three years of Fermi-LAT observations. Fermi has discovered and studied gamma-ray emission from around 100 pulsars,<sup>1</sup> more than two dozen of which are seen to pulse only in gamma-rays;<sup>2,3</sup> hundreds of AGN have been

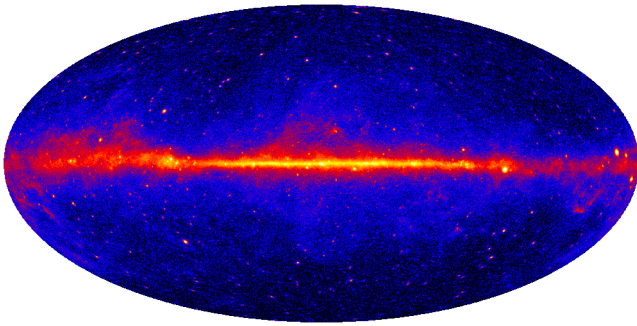


**Fig. 1** The gamma-ray sky above 1 GeV as seen by Fermi-LAT after three years of observations.

observed,<sup>4</sup> with unbiased and evenly sampled light curves<sup>5</sup>; more than 1800 sources are characterized in the recently released second LAT catalog,<sup>6</sup> and many hundreds of gamma-ray bursts have been signaled by the GBM to observatories worldwide<sup>7</sup>; important limits have been placed on fundamental physics parameters, including hypothesized tiny differences in the speeds of photons of vastly different energies,<sup>8</sup> and various particle models for the mysterious dark matter;<sup>9,10</sup> the electron and positron flux has been measured with vastly improved precision to 1 TeV;<sup>11,12</sup> giant gamma-ray “bubbles” have been discovered emanating from the center of our Galaxy;<sup>13</sup> the Crab supernova remnant—long considered to be a steady high-energy calibration source—has been found to be slowly decreasing in intensity over a broad energy range<sup>14</sup> as well as flaring dramatically on very short timescales,<sup>15</sup> challenging particle acceleration models; and antimatter (positrons) has been observed to be produced by terrestrial lightning flashes.<sup>16</sup> The prime mission phase for Fermi is five years but, as there are no consumables on the observatory and seemingly no end to the variability of the gamma-ray sky, as well as great interest in new faint source classes, the mission lifetime goal is 10 years.

The science requirements for the mission were developed by a Facility Science Definition Team for NASA, and they formed the basis for the instrument Announcement of Opportunity. The LAT and GBM teams were selected in this process, along with four interdisciplinary scientists who, together with representatives from the other mission elements, formed the Science Working Group (SWG). The SWG refined the science requirements.<sup>23</sup> The Observatory meets or exceeds all requirements.

## 2 Observatory

### 2.1 Large Area Telescope

Gamma-ray photons, in the energy range of the LAT, 20 MeV to over 300 GeV, are sufficiently energetic that their detection and measurement relies on the production of matter from electromagnetic energy instead of focusing via reflection or refraction as for lower-energy photons. The principle of operation for the LAT is illustrated in Fig. 2.

The LAT measures the tracks of the electron ( $e^-$ ) and positron ( $e^+$ ) that result when an incident  $\gamma$ -ray undergoes pair-conversion, preferentially in a thin, high-Z foil, and measures the energy of the subsequent electromagnetic

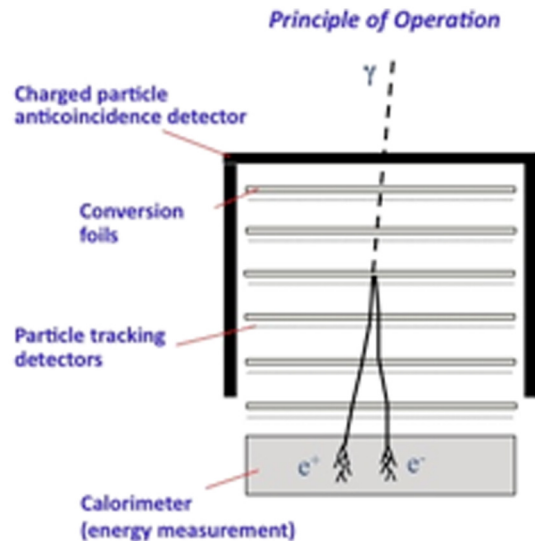


**Fig. 2** Principle of operation of the Large Area Telescope.

shower that develops in the telescope’s calorimeter.<sup>17</sup> The LAT is designed to measure the directions, energies, and arrival times of  $\gamma$ -rays incident over a wide Field of View (FoV), while rejecting background from cosmic rays.

The design approach made extensive use of detailed simulations of the detector response to signal ( $\gamma$ -rays from astrophysical sources) and backgrounds (cosmic rays, atmospheric  $\gamma$ -rays, etc.). The selected detector technologies used in the LAT experiment have an extensive history of application in space science and/or high-energy physics with demonstrated high reliability. Relevant test models were built to demonstrate that critical requirements—such as power, efficiency, and detector noise occupancy—could be met and these detector-system models, including all subsystems, were studied in accelerator test beams to validate both the design and the Monte Carlo programs used in the simulations. The modular design of the LAT allowed the construction, at reasonable incremental cost, of a full-scale, fully functional engineering demonstration telescope module for validation of the design concept.

The LAT consists of three detector subsystems, along with a flexible trigger and data processing system. A tracker/convertor (TKR), comprising 18 XY-layers of silicon-strip detectors (SSDs) with interleaved tungsten foils, measures the direction of incident particles, including  $\gamma$ -rays that convert in the tracker. A calorimeter (CAL), composed of 8.6 radiation lengths of CsI(Tl) scintillation crystal arranged hodoscopically in eight layers, provides energy measurements as well as some imaging capability that aids background rejection and energy reconstruction. An anti-coincidence detector (ACD), featuring an array of plastic scintillator tiles enclosed by a thermal blanket/micrometeoroid shield, surrounds the TKR and aids in the rejection of cosmic-ray backgrounds. The LAT has, by far, the largest particle tracker ( $\sim 70 \text{ m}^2$  of SSD’s, with 880,000 separate channels) and most massive calorimeter (1536 individual CsI crystals with total mass 1.5 tons) ever launched. The detectors, instrument power system, and the data system, which includes three active BAE RAD750 processors, in total dissipate less than 650 W.

The TKR and CAL each consist of a  $4 \times 4$  array of modules supported by a low-mass aluminum grid. A programmable trigger and data acquisition system utilizes prompt signals available from the TKR, CAL, and ACD subsystems to form a trigger. The self-triggering capability of the TKR is an important feature of the LAT design that is possible because of the choice of silicon-strip detectors, which do not require an external trigger, for the active elements. The hardware trigger rate varies over the orbit between 2 to 6 kHz. Onboard software reduces that rate by a factor 5 to 10 to fit within the 1.2 Mbps average data bandwidth allocation. The onboard processing is optimized for rejecting events triggered by cosmic-ray background particles while maximizing the number of events triggered by  $\gamma$ -rays, and it also provides a steady sample of events for calibration and monitoring. Heat produced by the TKR, CAL, and DAQ electronics is transferred through heat pipes in the grid to two spacecraft-mounted radiators.

The most important instrument performance parameters are shown in Fig. 3 and summarized in Refs. 17 and 24.

**LAT TKR:** The TKR is the subsystem of the LAT instrument where ideally the  $\gamma$ -rays convert to  $e^+e^-$  pairs and their trajectories are measured. A full description of the TKR can be found in Refs. 17 and 18. The TKR consists of 18 layers of paired  $X$ ,  $Y$  silicon-strip detector (SSD) planes. Starting from the top of the instrument (furthest from the CAL), the first 12 paired layers are arranged to

immediately follow “thin” converter foils, each  $\sim 3$  percent of a radiation length (RL) of tungsten. Minimizing the separation of the converter foils from the following SSD planes is critical for minimizing the effects of multiple scattering. This section of the TKR is sometimes referred to as the “thin” or “front” section. The next four layers are similar, except the thickness of the tungsten converters is  $\sim 6$  times larger (0.18 percent RL), and is referred to as the thick (or back) section. The last two layers have no converter and are needed to make-up the trigger for events converting in the last thick layer. There are notable differences in performance between the thin and thick TKR sections, especially the angular resolution and background contamination.

The inclusion of two different radiator thicknesses resulted from balancing the needs for high angular resolution required to pick apart complex regions of the sky, especially found on the Galactic plane, and for good overall event statistics (total effective area) which sets the temporal resolution accessible for transient events (the light curves). The radiators were chosen so that there are approximately the same numbers of events recorded in the thin and thick sections. In addition to these considerations, the aggregate of the thick layers (total thickness  $\sim 0.8$  RL) make the thin section events cleaner, with respect to background contamination, because the shielding by the thick foils limits both the amount of back-splash coming from the calorimeter in high-energy events as well as ranging out the tails of showers

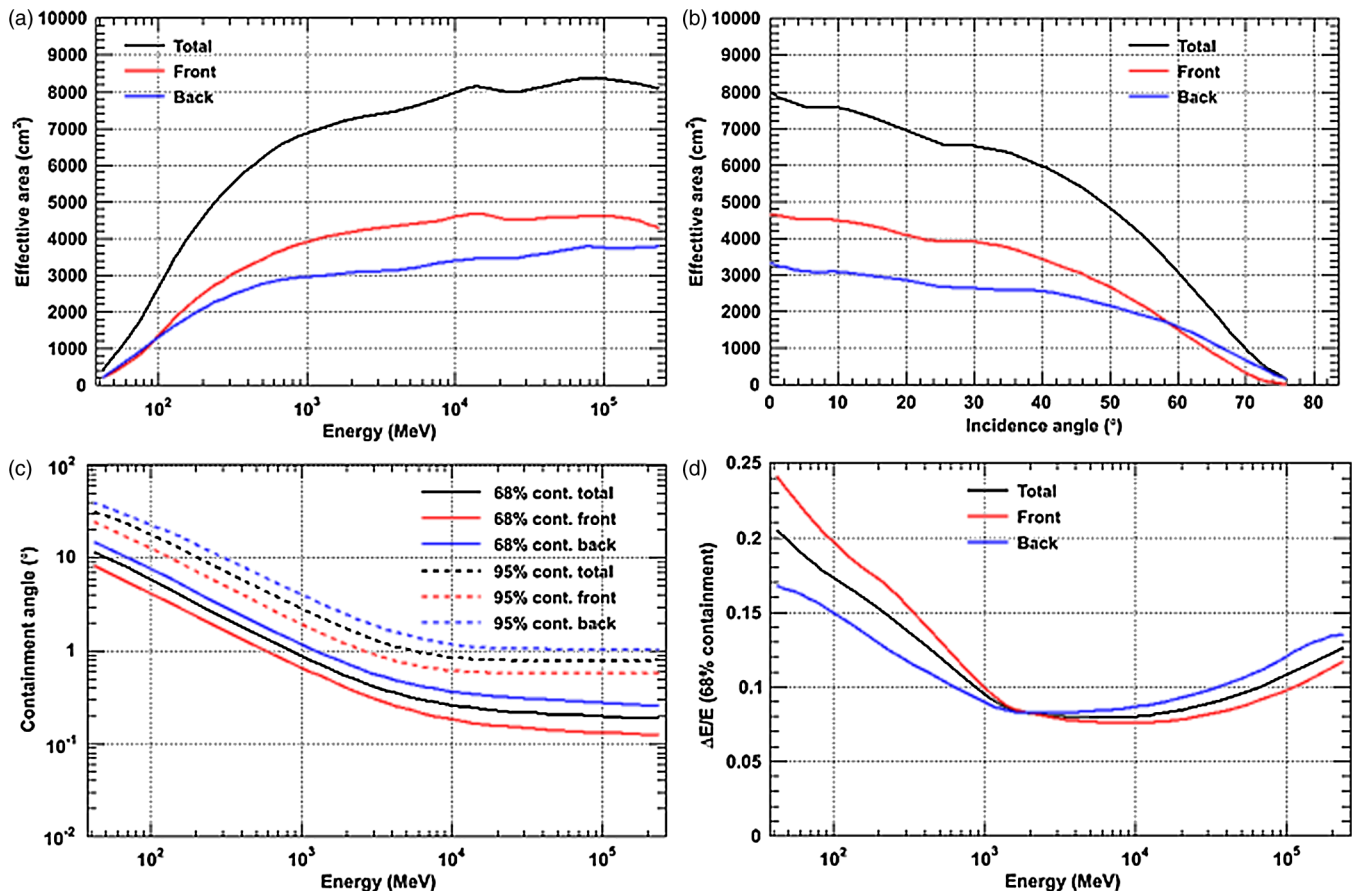


**Fig. 3** Fermi-LAT performance for the standard event selection recommended for point source analysis. The performance for gamma-rays which convert in the front (thin) part of the detector is shown separately to the back (thick) part of the detector. (a) Effective area as a function of energy. (b) Effective area as a function of incidence angle, illustrating the large field of view of Fermi-LAT. (c) Angular resolution (expressed as 68% and 95% containment radii) as a function of energy. (d) Energy resolution as a function of energy.

in the calorimeter from back-entering events. Figure 3 shows the angular resolution, effective area and energy resolution for events converting in the front (thin) and back (thick) sections of the tracker.

There are now three years of on-orbit experience with the TKR. The choice of the all-solid-state tracker technology (silicon strips) has resulted in negligible down time and extremely stable operation, minimizing the necessity for calibration measurements. The very high signal to noise provided by the front-end electronics has resulted in high single hit detection efficiency which, averaged over the entire TKR, is  $>99.8$  percent while the noise occupancy for the typical TKR readout channel remains  $<10^{-5}$ . The low noise occupancy and high efficiency has resulted in extremely high efficiency for finding tracks and has been key to providing the information necessary to reject backgrounds.

Perhaps the most important performance parameter for the TKR is the resulting point-spread-function (PSF) for reconstructed  $\gamma$ -ray directions. At low-energy the PSF is dominated by multiple scattering, primarily within the tungsten conversion foils (for the thin section  $\sim 67$  percent of material in each layer is tungsten, while for the thick layers it is  $\sim 92$  percent). The calculated multiple scattering for an ideal normal incidence 100 MeV  $\gamma$ -ray converting in the middle of a thin section tungsten foil is  $\sim 3.1^\circ$  (space angle). The performance as measured from flight data using point sources for 100 MeV  $\gamma$ -rays near the instrument axis averaged over all towers is  $\sim 3.3^\circ$ , in agreement with Monte Carlo calculations. The small difference between the simple analytic estimate and real data is due to missed track measurements that occur when the trajectories happen to pass through regions without SSD coverage, and the fact that the electron and positron from the conversion can undergo hard scattering processes such as bremsstrahlung. These effects are included in the Monte Carlo model of the instrument.

If multiple scattering were the only contribution, the PSF should improve at higher energy as  $E^{-1}$ . The measured PSF however improves more slowly with energy, instead falling as  $\sim E^{-0.8}$ . This slower improvement with energy over that expected for pure multiple scattering is, again, due to missed coordinates and the aforementioned hard scattering processes and is predicted by the Monte Carlo calculations.

Above a few GeV, the improvement in the PSF as the energy increases slows because the finite precision of the SSDs comes into play. The strip pitch of 228  $\mu\text{m}$  results in a limiting precision for the average conversion of  $\sim 0.1^\circ$  at normal incidence. The transition to this measurement precision dominated regime, as predicted by the instrument Monte Carlo model, should occur between  $\sim 3$  GeV and  $\sim 20$  GeV. Estimates of the limiting PSF from flight data, however, indicate a worse performance at high energies with the PSF asymptoting at almost double the calculated value ( $\sim 0.16^\circ$ ). This departure is one of the few instances where the Monte Carlo results differ significantly from real data and (needless to say) is under investigation.

**LAT CAL:** The CAL is a 3D imaging calorimeter (see Refs. 17 and 19 for a complete description). This is achieved by arranging the CsI crystals in eight layers and, within each CAL module, the width of each layer is spanned by 12 crystal “logs.” Alternating layers are rotated by  $90^\circ$ . Figure 4 shows a deconstructed view of the LAT calorimeter. Each

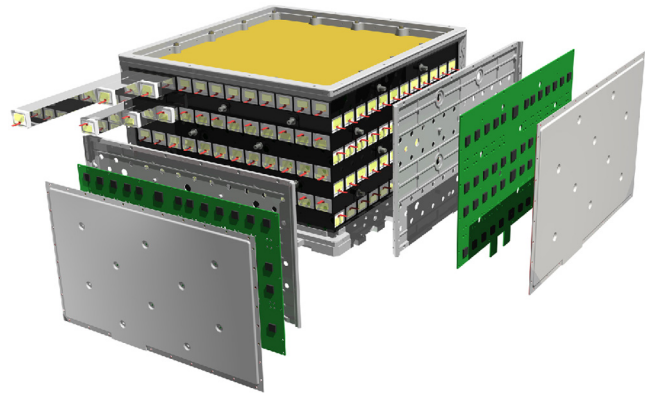


Fig. 4 The Fermi-LAT calorimeter.

log is read out from both ends using two photodiodes (a large one to cover low energies and a small one for high-energy), each of which has a low- and high-gain electronics channel; thus, the readout for each crystal end has four overlapping gain scales, covering a dynamic range of  $\sim 10^5$ . Each CsI crystal provides three spatial coordinates for the energy deposited within it: two discrete coordinates from the physical location of the crystal in the array and the third, more precise, coordinate determined by measuring the light yield asymmetry at the ends of the crystal along its long dimension. This level of segmentation is sufficient to allow spatial imaging of the shower and accurate reconstruction of its direction. The CAL's shower imaging capability and depth contribute significantly to background rejection, particularly of non-electromagnetic showers, as well as enabling an energy reconstruction that compensates event-to-event total energy fluctuations due to shower leakage either out the back or the sides of the CAL.

**LAT ACD:** The anti-coincidence detector (ACD) is critical for the identification of cosmic rays (as opposed to  $\gamma$ -rays). Details of its design can be found in Refs. 17 and 20. From experience with the previous large pair-conversion telescope, EGRET on CGRO,<sup>21</sup> it was realized that a high degree of segmentation to minimize “self veto” due to the back-splash of hard X-rays from showers in the CAL was required. Overall, the LAT ACD consists of 25 scintillating plastic tiles covering the top of the instrument and 16 tiles covering each of the four sides (89 in all). The segmentation of the ACD purposely does not match that of the LAT tower modules to avoid lining up gaps in ACD subsystem with those in the TKR and CAL. The design requirement for the ACD was to reject entering charged particles with an efficiency  $>99.97$  percent. To meet the efficiency requirement, very careful consideration as to light collection via wavelength shifting fibers, and meticulous attention in the fabrication to maintain the maximum light yield, was needed. The average light yield is  $\sim 23$  photo-electrons (p.e.) for each of the two redundant fiber readouts associated with each tile.

The necessary ACD segmentation inevitably led to hermeticity issues at odds with construction reality. The solution was to overlap scintillator tiles in one dimension, leaving gaps between tile rows in the other. To provide coverage of these 2 to 3 mm gaps, bundles of scintillating fibers, “Ribbons,” were used and readout at each end by a photo-multiplier tube (PMT). The light yield for these Ribbons ( $\sim 8$  p.e.), however, is considerably less than for the tiles

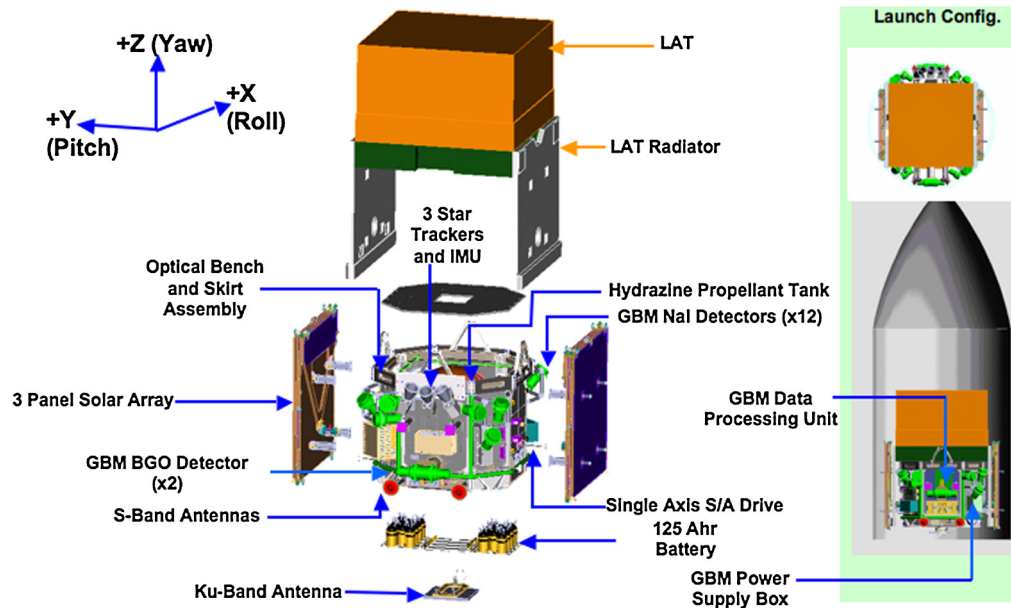


Fig. 5 Spacecraft configuration.

and varies along the length of the Ribbon. Hence, the gaps' efficiency for detecting the passage of charged particles is less than for the tiles. However, the gaps are a small fraction of the total area (<1 percent) and overall do not compromise the design requirement. In addition to the gaps between ACD tile rows, the corners on the sides of the ACD have gaps as well, which are taken into account in the reconstruction analysis.

## 2.2 Gamma-Ray Burst Monitor

The Gamma-ray Burst Monitor extends Fermi's capabilities and complements the LAT by providing observations of bright transient sources at lower energy  $\gamma$ -rays (8 keV to 40 MeV). The primary objective of the GBM is to extend the energy range over which  $\gamma$ -ray bursts are observed downward from the LAT range into the hard X-ray range where extensive previous data exist. A secondary objective is to compute burst locations onboard, which repoint the spacecraft to allow the LAT to observe delayed high-energy gamma-ray emission from these objects.

The GBM consists of 12 thin NaI(Tl) plates, which are sensitive in the energy range between 8 keV and  $\sim 1$  MeV, and two cylindrical BGO scintillation detectors which can detect gamma-rays in the energy range between 150 keV and 40 MeV. The axes of the NaI(Tl) detectors are oriented such that the positions of gamma-ray bursts can be derived from the measured relative counting rates. A detailed description of the GBM can be found in Meegan et al.<sup>22</sup>

The NaI(Tl) detectors are composed of cylindrical crystal disks, with a diameter of 12.7 cm and thickness of 1.27 cm. They are packed in a hermetically sealed light-tight aluminum housing with a 0.6 cm glass window. The radiation-entrance window of the NaI detectors is composed of a 0.22-mm-thick Be sheet for good response at low energies, but for mechanical reasons a 0.7-mm-thick silicone layer was placed in front of the crystals, which primarily determines the low-energy threshold of 8 keV.

The BGO detectors are cylinders of 12.7 cm diameter and 12.7 cm length. The two circular side windows are polished to mirror quality, while the cylindrical surface is roughened to guarantee diffuse reflection of the generated photons. Both the BGO and NaI(Tl) detectors are coupled to Hamamatsu R877-MOD photomultiplier tubes to convert the scintillation light to an electric signal.

A burst trigger occurs when the GBM flight software detects an increase in the count rates of two or more NaI detectors above an adjustable threshold specified in standard deviations above background.

The GBM determines the location of the  $\gamma$ -ray burst by determining the relative count rates in the various NaI detectors and comparing this to a table of calculated relative count rates for each of 1634 directions ( $\sim 5$  deg resolution). The initial location is calculated onboard within 1.8 s, yielding an accuracy of around  $15^\circ$ .

The probability that the trigger event is a  $\gamma$ -ray burst as opposed to a solar flare, particle precipitation event or known transient source is calculated onboard using a Bayesian approach that includes the event coordinates, the spectral hardness and the spacecraft geomagnetic coordinates.

## 2.3 Spacecraft

The spacecraft bus was designed, built, and tested by General Dynamics Advanced Information Systems\* (GD-AIS), which also provided Observatory integration and testing. The core bus was competitively awarded through the Rapid Spacecraft Development Office (RSDO) at GSFC.

The spacecraft bus comprises the standard elements on most NASA satellites: command and data handling (CDH), guidance, navigation and control (GNC), communications (COMM), electrical power system (EPS), thermal control

\*The fixed price contract was awarded to Spectrum Astro Space Systems (SASS) of Gilbert AZ in 2002. General Dynamics bought SASS in 2005, but spacecraft development continued in Gilbert.

system (TCS), flight software (FSW), propulsion (Prop), and structure (Fig. 5).

The structure is primarily aluminum, with four titanium flex supports for the LAT. Most of the components are externally mounted, with the propulsion tank and reaction wheels mounted inside.

The CDH comprises 18 boards, plus a 160-Gbit solid-state recorder (SSR) and two oven-controlled crystal oscillators. The CDH is block redundant. The SSR is partitioned into two sections: one for LAT and GBM science data and one for spacecraft and instrument housekeeping data. The interface from the GBM and LAT to the recorder is LVDS (Low Voltage Differential Signal) and data transfer rates can be as high as 44 Mbps. The CPU is a BAE RAD 750 with a cPCI bus. The nominal housekeeping rate is 51 Kbps for both instruments and the spacecraft bus.

The COMM system comprises two multi-mode S-band transmitters (SMA and SSA), two Ku-band transmitters, a Ku-band antenna and pointing control system, and four omni-directional antennas. SSA downlink rates are 1, 2, 4, and 8 Kbps to TDRSS, and 2.5 Mbps to the ground stations. The Ku-band transmitter output rate is 40 Mbps. The Ku-band antenna pointing assembly is used to point the antenna to a TDRS (Tracking and Data Relay Satellite) and maintain track during Ku-band contacts. Commanding is done primarily through TDRSS with a 4 Kbps uplink rate for SSA and a 250 bps uplink rate for MA.

The EPS is composed of two solar arrays, each with its own drive electronics, a single 125-AH battery, charge and discharge control mechanisms, and a power regulation unit that provides 28 volts  $\pm 1$  volt to the LAT. It provides enough power in daylight to recharge the battery and keep the instruments and spacecraft components operating.

The GNC system is a zero-momentum-biased system and is 3-axis stabilized. Four reaction wheel assemblies (RWAs) are used for slewing and momentum management. The pointing and slewing requirements can be met with just three wheels operating. Torque rods are used for unloading momentum. Two active CCD star trackers are used for attitude determination. A third unit is a cold spare. The hemispherical resonant gyro (HRG) provides rate information and is internally redundant. The spacecraft receives time and position data from the GPS constellation for use by the GNC and the instruments.

The TCS provides active and passive thermal control. Radiators are used for the battery and other elements. The battery operates with a flight software (FSW)-controlled thermostat, backed up by redundant survival heaters. Heat pipes are also used to provide a stable on-orbit thermal environment.

Spacecraft FSW controls the operations of the bus for both the normal functionality (commutating data, limit checking, safeing protection) and for controlled reentry at end of mission.

The Prop system has two purposes: controlled reentry and collision avoidance. Because some observatory debris will survive reentry, the de-orbit is controlled. The Propulsion system also enables small maneuvers ( $\sim$  few-second burns) to avoid possible collisions with monitored on-orbit debris from other space-based activities. (Such collision avoidance maneuvers have so far not been necessary.) Twelve 5-lb

thrusters and a tank containing approximately 350 kg of hydrazine are for these two functions.

### 3 Mission Operations and Observing Modes

#### 3.1 Launch and Early Operations

On June 11, 2008, Fermi was launched into a circular low earth orbit, with an inclination of  $25.6^\circ$  and an altitude of 565 km, aboard a Delta II heavy rocket.

The first 14 days were primarily spent turning on and calibrating the attitude control system and tuning the EPS. Instrument commissioning began on day 14, when both LAT and GBM were switched on. The next four weeks were spent calibrating and optimizing the configuration of the LAT and GBM instruments. Science operations began on August 4, one week ahead of schedule.

#### 3.2 Observing Modes

The primary observing pattern for Fermi is an all-sky survey. In this mode, the spacecraft sweeps the  $z$ -axis across the sky at a specified angle perpendicular to the orbit plane. The survey mode profile is specified as a sequence of 17 waypoints (angle and time pairs), allowing significant flexibility in the survey pattern. The current profile rocks above the orbit plane by  $50^\circ$  for one orbit and below the orbit plane by  $50^\circ$  on the next orbit, this pattern repeats while survey mode continues. With the large field of view of the LAT, the current survey profile provides complete coverage of the sky every two orbits, or just over 3 hours.

Fermi can also execute inertially pointed observations to maximize coverage of a source during a specified period of time. This provides a capability to monitor the source to greater accuracy and to shorter timescales than would be possible in survey mode.

There are three types of pointed mode observations:

1. Planned observations which are scheduled weeks before,
2. Target of opportunity (TOO) which are manually commanded as soon as possible after a request comes in, and
3. Autonomous repoints (ARs) which are performed autonomously by the spacecraft after a bright LAT or GBM-detected gamma-ray burst (Sec.3.3).

The Fermi observatory can safely point the spacecraft  $z$ -axis (the direction of the LAT boresight) anywhere at any time, including at the Earth. However, to maintain observing efficiency, it is advantageous to minimize the fraction of the LAT field of view that is occulted by the Earth. How this is achieved depends on the way the observation was scheduled.

In preplanned pointed mode observations, the FSSC usually schedules a small slice of survey mode each orbit during periods when the target location is behind the earth. Thus, the observation is commanded as a sequence of pointed mode and survey mode observations. When only a single target is commanded (typically during target of opportunity or autonomous repoints) the spacecraft automatically avoids pointing at the earth in the following way. As the target approaches occultation, the spacecraft continues tracking until it gets to the Earth Avoidance Angle (EAA) to the earth's limb (currently set to  $5^\circ$ ). The spacecraft

**Table 1** Observations between August 2008 to July 2011. The observatory spends most of the time in sky survey mode with a small fraction of time in pointed mode (either ARR or TOO). The observatory efficiency is very high, with less than 1 percent of time devoted to engineering or calibration activities.

	Sky Survey	ARR	TOO/pointed	Engineering
2008	99.3%	0.4%	0%	0.3%
2009	97%	1.7%	0%	1.3%
2010	97.4%	0.9%	1.6%	0.1%
2011	93%	0.4%	6.2%	0.2%

remains at this angle from the earth limb until the target passes behind the earth. At this time, the spacecraft slews around the edge of the earth, stepping out to a larger angle from the earth (currently)  $50^\circ$  before coming back to the other side of the earth to pick up the target, arriving one EAA from the earth limb just as the target emerges from occultation. The fraction of time that the observatory is in each observation mode is tabulated in Table 1.

### 3.3 Gamma-Ray Burst Handling

Gamma-ray bursts (GRB) are intense transient bursts (typically a few seconds in duration) of  $\gamma$ -rays from random locations on the sky. These observations require special handling to maximize the science return for several reasons:

1. it is important to determine a burst location and relay that location to other observatories as quickly as possible to allow rapid follow up observations at lower energies,
2. we want to maximize the time that the GRB is within the LAT FoV for the first few hours after the burst, to allow a sensitive search for high-energy afterglows.

Both the LAT and the GBM perform onboard searches for gamma-ray bursts. When either instrument detects a burst, the observatory uses the Demand Access System (DAS) on TDRSS to autonomously relay a burst alert notice. The TDRSS DAS system allows the spacecraft to transmit these messages to the ground system without having to schedule specific contacts. These notices are then circulated by the Gamma-ray burst Coordinates Network (GCN) to observatories around the world. The initial notice is followed by messages with localizations calculated by the flight software of each detector. Additional data (burst and background rates) are also sent down by the GBM through TDRSS for an improved rapid localization on the ground by a dedicated processor. The first burst location message is typically received by GCN and disseminated within 15 seconds of the onset of the GRB.

The spacecraft can autonomously slew to bring the GRB location to the center of the LAT field of view for several hours, enabling continuous high-sensitivity LAT observations interrupted only by South Atlantic Anomaly (SAA) passages and when the target location is occulted by the earth. The rate of GBM-detected transients is sufficiently large enough that repointing to every GRB would cause

significant disturbance to science studies that depend on regular survey mode operations. To mitigate this, the GBM flight software evaluates the flux, fluence and spectral properties of each GRB to select the subset deemed most scientifically interesting for pointed mode observations. A repoint recommendation from GBM is sent to the LAT at the time the GBM repoint criteria are met. The LAT forwards the repoint request to the spacecraft using a LAT localized position if one is available, and otherwise uses the GBM-determined location in the repoint request to the spacecraft.

### 3.4 Routine Operations and Data Handling

The Fermi ground system is composed of several major elements. The Mission Operation Center provides the basic command and control of the observatory and performs level 0 processing for LAT and GBM data. The LAT and GBM ground systems perform level 1 and 2 data processing, instrument calibration, and instrument planning and scheduling. The NASA Space Network is used to downlink the data and provide a conduit for commanding. The FSSC provides long-term storage of level 0 to 2 products and integrates the mission timeline.

FSW and stored commands are loaded from the MOC on a weekly basis as the primary control of the spacecraft. The MOC schedules the Space Network (aka: TDRSS) to downlink the stored science and engineering data. The stored command capability is used to autonomously play back the data via the Ku-band link approximately 12 times per day, for a total of approximately 100 minutes. This is equivalent to an average data rate of a little over 1.5 Mbps, with all but a small portion being generated by LAT. The FSW manages the Ku-band antenna to position it prior to playback and place it in a fixed position after the playback ends.

From the beginning of science operations in August 2008 until July 2011, the LAT has read out over 200 billion events, of which more than one hundred million have been flagged as  $\gamma$ -rays and sent to the FSSC. The GBM FSW triggered on 1194 transient sources at MeV energies (including 654 Gamma-Ray Bursts, 141 Terrestrial Gamma-ray Flashes, 174 Soft Gamma-ray Repeater flares and 56 solar flares). The observatory has performed 66 ARRAs following the onboard detection of bright gamma-ray bursts. The FSSC has served over 10 TB of data to the scientific community.

## 4 Science Analysis Support and Data Products

The Fermi mission has three phases after launch:

- Phase 0: the  $\sim 60$  days after launch when the instruments were turned on and calibrated.
- Phase 1: the first year of scientific operations. The instrument teams continued to calibrate their instruments while conducting a sky survey.
- Phase 2: the rest of the mission

The Fermi mission entered Phase 2 on August 4, 2009. During Phase 2, Fermi data are available to the scientific community as soon as the required Level 1 processing preparing the data for scientific analysis has been performed and the resulting Level 1 data have been transmitted to the FSSC. This processing is almost always completed within a day after the Level 0 data arrive at the Level 1 pipeline at the IOCs. The SSC loads the Level 1 data into the public

databases within a day after it receives these data. Once the data are loaded into the FSSC databases, they are publicly available to all scientists and the general public. There is no proprietary period for data.

Analysis of data from the Fermi instruments is supported by software available from the FSSC, together with detailed documentation and analysis threads that describe typical analysis procedures. The data, software, and documentation are all available through the FSSC.<sup>25</sup>

The Fermi Guest Investigator Program provides funding for direct analysis of Fermi data, for supporting observations in other wavebands, for complementary theoretical studies, and more. The deadline for proposals is typically in January every year. The FSSC maintains an accurate, timely, and publicly available list of accepted investigations.

## 5 A Look Ahead

The first three years of Fermi observations have provided the deepest-ever image of the whole  $\gamma$ -ray sky, uncovering hundreds of new  $\gamma$ -ray sources and, more importantly, new classes of  $\gamma$ -ray sources. Fermi's continuous monitoring provides exquisite time histories of the  $\gamma$ -ray behavior of all objects on the sky—allowing a uniquely detailed study of known variable objects such as active galaxies, the observation of intense flares from objects previously presumed to be steady such as the Crab Nebula, to the discovery of  $\gamma$ -rays from phenomena not initially expected to produce  $\gamma$ -rays such as the nova in V407 Cyg.

There is much still to do—in the time domain, longer observations allow us to explore phenomena that occur on long timescales such as potential yearly quasi-periodic signatures from supermassive binary black holes in AGN. As Fermi collects more data, the view of the  $\gamma$ -ray sky will get deeper and deeper, uncovering new classes of  $\gamma$ -ray sources. The detection of more members of known source classes will allow study of the properties of populations of  $\gamma$ -ray bright source classes in order to uncover the fundamental principles behind these enigmatic sources. The energy range covered by Fermi-LAT increases to higher energies with longer observations, owing to the very low celestial fluxes at the highest energies, opening up new discovery space. This higher energy coverage will be complementary to the next generation of ground-based air (CTA) and water (HAWC) Cherenkov telescopes.

As new multi-wavelength survey instruments such as Pan-STARRS, LSST, HAWC, LOFAR, Planck, WISE, and multi-messenger facilities such as Advanced-LIGO and ICECUBE come online or are completed, the opportunity for cross discovery of completely new processes in known objects and new previously unknown source classes is exciting and unprecedented. Detections of neutrino or gravitational wave transient sources will require verification with electromagnetic observations and comparisons to known phenomena. Fermi's all-sky capabilities and window into the most violent processes in the universe will help facilitate these discoveries by providing a vital piece of the puzzle to help localize, identify, and understand these objects.

As the community continues to utilize Fermi and dream up new data analyses and observations, Fermi will remain the versatile facility that has already led to so many unexpected discoveries. It will undoubtedly continue to reveal more surprises for years to come.

## Acknowledgments

We thank our colleagues—scientists, engineers, technicians, and staff—around the world who worked together on the design, construction and operation of the Fermi Observatory. The mission would not have happened without them. We also thank Bill Atwood, Dave Thompson, Judy Racusin, and Jack Leibee for their inputs to this paper. The Fermi LAT Collaboration acknowledges generous ongoing support from a number of agencies and institutes that have supported both the development and the operation of the LAT as well as scientific data analysis. These include the National Aeronautics and Space Administration and the Department of Energy in the United States, the Commissariat à l'Energie Atomique and the Centre National de la Recherche Scientifique / Institut National de Physique Nucléaire et de Physique des Particules in France, the Agenzia Spaziale Italiana and the Istituto Nazionale di Fisica Nucleare in Italy, the Ministry of Education, Culture, Sports, Science and Technology (MEXT), High-Energy Accelerator Research Organization (KEK) and Japan Aerospace Exploration Agency (JAXA) in Japan, and the K. A. Wallenberg Foundation, the Swedish Research Council and the Swedish National Space Board in Sweden. Additional support for science analysis during the operations phase is gratefully acknowledged from the Istituto Nazionale di Astrofisica in Italy and the Centre National d'Etudes Spatiales in France. The Fermi GBM collaboration acknowledges support for GBM development, operations and data analysis from NASA in the U.S. and BMWi/DLR in Germany.

## References

1. A. A. Abdo et al., "The first Fermi Large Area Telescope catalog of gamma-ray pulsars," *Astrophys. Suppl. J.*, **187**, 460–494 (2010).
2. A. A. Abdo et al., "Detection of 16 Gamma-Ray Pulsars Through Blind Frequency Searches Using the Fermi LAT," *Science*, **325**, 840 (2009).
3. P. M. Saz Parkinson et al., "Eight  $\gamma$ -ray pulsars discovered in blind frequency searches of Fermi LAT data," *Astrophys. J.*, **725**, 571 (2010).
4. A. A. Abdo et al., "The first catalog of active galactic nuclei detected by the Fermi Large Area Telescope," *Astrophys. J.*, **715**, 429–457 (2010).
5. A. A. Abdo et al., "Gamma-ray light curves and variability of bright fermi-detected blazars," *Astrophys. J.*, **722**, 520–542 (2010).
6. A. Goldstein et al., "The Fermi GBM gamma-ray burst spectral catalog: the first two years," ArXiv e-prints, arXiv:1201.2981 (2012).
7. W. B. Paciesas et al., "The Fermi GBM gamma-ray burst catalog: the first two years," ArXiv e-prints, arXiv:1201.3099 (2012).
8. A. A. Abdo et al., "A limit on the variation of the speed of light arising from quantum gravity effects," *Nature*, **462**, 331–334 (2009).
9. A. A. Abdo et al., "Fermi Large Area Telescope search for photon lines from 30 to 200 GeV and dark matter implications," *Phys. Rev. Lett.*, **104**(2), 091302 (2010).
10. A. A. Abdo et al., "Observations of milky way dwarf spheroidal galaxies with the Fermi-Large Area Telescope detector and constraints on dark matter models," *Astrophys. J.*, **712**, 147–158 (2010).
11. A. A. Abdo et al., "Measurement of the cosmic ray  $e^+e^-$  measurement of the cosmic ray spectrum from 20 GeV to 1 TeV with the Fermi Large Area Telescope," *Phys. Rev. Lett.*, **102**, 181101 (2009).
12. M. Ackerman et al., "Fermi LAT observations of cosmic-ray electrons from 7 GeV to 1 TeV," *Phys. Rev. D*, **82**(9), 092004 (2010).
13. M. Su, T. R. Slatyer, and D. P. Finkbeiner, "Giant gamma-ray bubbles from Fermi-LAT: active galactic nucleus activity or bipolar galactic wind?" *Astrophys. J.*, **724**, 1044–1082 (2010).
14. C. A. Wilson-Hodge et al., "When a standard candle flickers," *Astrophys. Lett. J.*, **727**, 40 (2011).
15. A. A. Abdo et al., "Science," "Gamma-ray flares from the crab nebula," **331**, 739 (2011).
16. M. S. Briggs, "Electron-positron beams from terrestrial lightning observed with Fermi GBM," *Geophys. Res. Lett.*, **38**(2), 2808 (2011).
17. W. B. Atwood et al., "The Large Area Telescope on the Fermi gamma-ray space telescope mission," *Astrophys. J.*, **697**, 1071–1102 (2009).
18. W. B. Atwood et al., "Design and initial tests of the tracker-converter of the gamma-ray large area space telescope," *Astropart. Phys.*, **20**, 422–434 (2007).
19. J. E. Grove and W. N. Johnson, "The calorimeter of the Fermi Large Area Telescope," *Proc. SPIE*, **7732**, 77320J (2010).

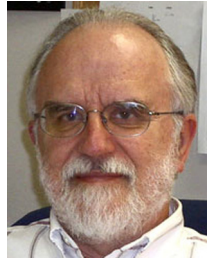
20. A. Moiseev et al., "The anti-coincidence detector for the GLAST Large Area Telescope," *Astropart. Phys.*, **27**, 339–358 (2007).
21. D. J. Thompson et al., "Calibration of the energetic gamma-ray experiment telescope (EGRET) for the Compton gamma-ray observatory," *Astrophys. Suppl. J.*, **86**, 629–656 (1993).
22. C. Meegan et al., "The Fermi gamma-ray burst monitor," *Astrophys. J.*, **702**, 791–804 (2009).
23. Available at [http://fermi.gsfc.nasa.gov/science/433-SRD-0001\\_CH-04.pdf](http://fermi.gsfc.nasa.gov/science/433-SRD-0001_CH-04.pdf).
24. [http://www-glast.slac.stanford.edu/software/IS/glast\\_lat\\_performance.htm](http://www-glast.slac.stanford.edu/software/IS/glast_lat_performance.htm).
25. <http://fermi.gsfc.nasa.gov/ssc/>.



**Julie McEnery** is an astrophysicist at Goddard Space Flight Center and adjunct associate professor at the University of Maryland, College Park. She has served as the project scientist for the Fermi mission since April 2009.



**Dr. Peter Michelson** is a professor of Physics at Stanford University and principal investigator for the Fermi Large Area Telescope. He is the co-recipient (along with William Atwood and the LAT team) of the 2011 Rossi Prize of the AAS.



**William S. Paciesas** received his BS from Seton Hall University in 1969 and his MS and Ph.D. from the University of California, San Diego in 1971 and 1978, respectively. He was an NAS/NRC resident research associate at NASA Goddard Space Flight Center from 1978 to 1980, and a research associate at the University of Maryland from 1980 to 1982. Since 1982 he has been a member of the research faculty at the University of Alabama in Huntsville and has served as associate director of the Center for Space Plasma and Aeronomic Research at UAHuntsville since 2004. He is currently Principal Investigator for the Fermi Gamma-ray Burst Monitor. His research interests include observational high-energy astrophysics, especially gamma-ray bursts, as well as terrestrial gamma-ray flashes.



**Steve Ritz** is Professor of Physics and Director of the Santa Cruz Institute for Particle Physics at the University of California Santa Cruz. He was the Fermi Project Scientist during most of the pre-launch development and the first year of science operations. He continues in several roles on Fermi, including LAT Deputy Principal Investigator.